

The very short-lived ozone depleting substance CHBr_3 (bromoform): Revised UV absorption spectrum, atmospheric lifetime and ozone depletion potential

D. K. Papanastasiou,^{1,2}& S. A. McKeen,^{1,2} and J. B. Burkholder^{1,*}

¹ Earth System Research Laboratory, Chemical Sciences Division, National Oceanic and Atmospheric Administration, 325 Broadway, Boulder, CO 80305, USA

² Cooperative Institute for Research in Environmental Sciences, University of Colorado, Boulder, CO 80309, USA

Running Title: Atmospheric lifetime of CHBr_3

Keywords: CHBr_3 , bromoform, absorption spectrum, UV, atmospheric photolysis, lifetime, ozone depletion potential

& Current address: Institute of Chemical Engineering and High Temperature Chemical Processes (ICE-HT), Foundation for Research and Technology Hellas (FORTH), Patras, 26504, Greece

* Correspondence to: James B. Burkholder; e-mail: James.B.Burkholder@noaa.gov

Abstract

CHBr₃ (bromoform) is a short-lived atmospheric trace compound that is primarily of natural origin and is a source of reactive bromine in both the troposphere and stratosphere. Estimating the overall atmospheric impact of CHBr₃ and its transport to the stratosphere requires a thorough understanding of its atmospheric loss processes, which are primarily UV photolysis and reaction with the OH radical. In this study, UV absorption cross sections, $\sigma(\lambda, T)$, for CHBr₃ were measured at wavelengths between 300 and 345 nm at temperatures between 260 and 330 K using cavity ring-down spectroscopy. The present results are compared with currently recommended values for use in atmospheric models and the discrepancies are discussed. A parameterization of the CHBr₃ UV spectrum for use in atmospheric models is developed and illustrative photolysis rate calculations are presented to highlight the impact of the revised $\sigma(\lambda, T)$ values on its calculated local lifetimes, e.g. the photolysis rate in the tropical region obtained with the present spectral data is 10–15% lower (longer lifetime) than obtained using currently recommended cross section values. Seasonally dependent ozone depletion potentials (ODPs) for CHBr₃ emitted in the Indian sub-continent were calculated to be 0.08, 0.26, 0.54, and 0.17 (Winter, Spring, Summer, Fall) using the semi-empirical relationship of Brioude et al. (*Brioude et al., Geophys. Res. Lett.*, 37, L19804, doi: 10.1029/2010GL044856, 2010).

1. Introduction

CHBr₃ (bromoform) is a short-lived atmospheric trace gas primarily emitted from natural sources such as marine phytoplankton and coastal macrophytes (seaweeds), and represents a source of reactive bromine (Br_y; Br + BrO) in the troposphere as well as the stratosphere. The atmospheric abundance of CHBr₃ in the marine boundary layer (MBL) has been measured to be in the range 0.5 to 2.4 ppt and the abundance in the upper tropical-tropopause layer to be in the range 0.01 to 0.29 ppt (WMO [2011] and references cited within). The transport of short-lived brominated species, and their brominated degradation products, to the stratosphere is known to impact stratospheric ozone. Brominated compounds are particularly impactful due to the high efficiency of stratospheric catalytic ozone destruction cycles involving bromine; bromine is estimated to be ~60 times more efficient in ozone destruction than chlorine (WMO, 2011). Current best estimates are that very short-lived substances (VSLs) contribute 3 to 8 ppt to the stratospheric bromine budget; the total stratospheric bromine abundance in 2008 was estimated to be ~22 ppt (WMO, 2011). In recent modeling studies, Hossaini et al. (2010) and Aschmann and Sinnhuber (2013) estimate that CHBr₃ accounts for ~0.7 ppt of stratospheric bromine; ~50% from the CHBr₃ source gas and the remainder from product gas injection of bromine containing degradation products. Modeling the impact of CHBr₃ on stratospheric ozone, particularly in a changing climate, requires not only a thorough understanding of its emissions, but also its atmospheric loss processes. The primary atmospheric loss processes for CHBr₃ are UV photolysis and reaction with the OH radical (WMO, 2011). Loss rates (lifetimes) of CHBr₃ occur on timescales shorter, or comparable, to the time scales for atmospheric circulation and are, therefore, dependent on the location and season of emission as well as the local conditions (e.g. UV flux, OH radical abundance, and temperature). UV photolysis is thought to be the predominant atmospheric loss process for CHBr₃ with photolysis lifetimes on the order of 10s of days in the Tropics. A recent kinetic study has reported an OH + CHBr₃ reaction rate coefficient that is greater than used in previous modeling estimates of the CHBr₃ lifetime, implying a shorter lifetime with respect to the OH reaction (Orkin et al., 2013), and shorter overall lifetime. The focus of the present work was on obtaining improved CHBr₃ UV absorption cross section data for wavelengths (λ) in the actinic region, greater than 290 nm, that will lead to a refinement of its atmospheric photolysis rate and lifetime and, thus, its ozone depletion potential (ODP).

There are two studies of the CHBr₃ UV absorption spectrum currently available in the literature that are relevant to its atmospheric photolysis, i.e. in the wavelength region >290 nm. Gillotay et al. (1989) reported CHBr₃ spectra based on absorption cross section, $\sigma(\lambda, T)$, data measured between 170 and 310 nm at temperatures (T) in the range 240 to 295 K. The CHBr₃

spectrum exhibits evidence for several overlapping diffuse electronic transitions in this region with monotonically decreasing $\sigma(\lambda,T)$ at wavelengths >270 nm. Moortgat et al. (1993) subsequently reported CHBr_3 spectra between 286 and 362 nm, which extended the wavelength range coverage further into the more relevant atmospheric photolysis region. Moortgat et al. reported CHBr_3 spectra at several temperatures between 256 and 296 K and a $\sigma(\lambda,T)$ parameterization for use in atmospheric models. The agreement between the Gillotay et al. and Moortgat et al. cross section data sets at 298 K for the wavelengths common to both studies, 286 to 310 nm, is reasonably good with agreement to better than $\pm 5\%$. However, at the longer wavelengths of the Moortgat et al. study, the measurements were reported to be subject to possible systematic error due to possible sample impurities, e.g. Br_2 , and possible adsorption of CHBr_3 on the windows of the absorption cell. Sander et al. (2011) recommends the results from the Moortgat et al. study, the only study available that provides data in the critical wavelength region, for use in atmospheric model calculations.

There are several experimental and theoretical studies of the UV photolysis dynamics and quantum yields of CHBr_3 (Bayes et al., 2003; Huang et al., 2004; Peterson and Francisco, 2002; Xu et al., 2002) available in the literature that are also relevant to its atmospheric photochemistry. In an experimental study, Bayes et al. (2003) reported Br atom quantum yields in the photolysis of CHBr_3 at 266 nm and over the wavelength range 303 to 324 nm; the threshold for the dissociation of CHBr_3 to $\text{CHBr}_2 + \text{Br}$ photoproducts is 436 nm. They reported a decrease in the Br atom quantum yield at the longer wavelengths included in their study and suggested that this may be a consequence of a systematic error in the $\sigma(\lambda,298 \text{ K})$ values used in their data analysis, which were taken from Moortgat et al. (1993); the Br atom quantum yield was expected to be unity at the wavelengths most critical to atmospheric photolysis, <350 nm (Peterson and Francisco, 2002). Due to this discrepancy, as well as, the desire for accurate calculations of the CHBr_3 atmospheric photolysis rate (lifetime) and its impact on stratospheric ozone, additional measurements of the CHBr_3 UV absorption spectrum at wavelengths ≥ 300 nm are warranted.

An objective of the present work was to measure the UV absorption spectrum of CHBr_3 at wavelengths ≥ 300 nm, the region critically important to tropospheric photolysis but a region for which there is limited experimental data. Absorption cross sections, $\sigma(\lambda,T)$, for CHBr_3 were measured using cavity ring-down spectroscopy between 300 and 345 nm at seven temperatures in the range 260 to 330 K. On the basis of our work, a CHBr_3 $\sigma(\lambda,T)$ parameterization was developed for use in atmospheric models. The present results are compared with the previous

work of Moortgat et al. (1993) and the discrepancies are quantified and discussed. The overall impact of the revised $\sigma(\lambda, T)$ values was further quantified using calculations of the CHBr_3 atmospheric photolysis rate (local lifetime) and its semi-empirical ODP.

2. Experimental Details

UV absorption cross sections, $\sigma(\lambda, T)$, for CHBr_3 were measured using cavity ring-down spectroscopy (CRDS) at 5 nm increments over the range 300 to 345 nm. Measurements were performed at room temperature, 296 K, as well as at three lower and higher temperatures covering a range from 260 to 330 K. Due to measurement sensitivity and CHBr_3 vapor pressure limitations, our $\sigma(\lambda, T)$ measurements were limited to values greater than $\sim 7 \times 10^{-24} \text{ cm}^2 \text{ molecule}^{-1}$, which includes the wavelength range most critical for atmospheric photolysis. Measurements at temperatures $< 296 \text{ K}$ were performed over a more limited wavelength range due primarily to limitations imposed by the CHBr_3 vapor pressure temperature dependence.

The apparatus, which is described in greater detail elsewhere (Feierabend et al., 2009; Papanastasiou et al., 2013), included (1) two independent cavity ring-down cells, (2) a frequency doubled Nd:YAG pumped dye laser used to generate a tunable CRDS probe beam between 300 and 345 nm, (3) a frequency doubled Nd:YAG laser, 532 nm, (4) a UV absorption setup at 253.7 nm for the online measurement of the CHBr_3 concentration, and (5) gas flow and pressure measurement components. Key elements of the experimental apparatus and methods used are described briefly below.

In the CRDS technique (O'Keefe and Deacon, 1988), the absorption coefficient, $\alpha(\lambda)$, of a sample is determined from a measurement of ring-down time constants, $\tau(\lambda)$ and $\tau_0(\lambda)$, with and without a sample present, respectively,

$$\alpha(\lambda) = [\text{CHBr}_3] (\sigma(\lambda, T) + \sigma_R(\lambda)) = \frac{1}{c} \frac{d}{L_{\text{Abs}}} \left(\frac{1}{\tau(\lambda)} - \frac{1}{\tau_0(\lambda)} \right) \quad (\text{I})$$

where $\sigma_R(\lambda)$ is the CHBr_3 Rayleigh scattering cross section, d is the cavity pathlength, L_{Abs} is the pathlength of the sample, and c is the speed of light. $\sigma_R(\lambda)$ is defined as

$$\sigma_R(\lambda) = \frac{32\pi^3}{3\lambda^4 N^2} (n - 1)^2 \quad (\text{II})$$

where N is Loschmidt's number and n is the index of refraction of CHBr_3 . $\sigma_R(\lambda)$ values for CHBr_3 in the wavelength range from 300 to 345 nm are relatively small compared to $\sigma(\lambda, T)$, e.g. $(1-4) \times 10^{-24} \text{ cm}^2 \text{ molecule}^{-1}$ (as determined in this work). However, accounting for $\sigma_R(\lambda)$ is required for an accurate determination of $\sigma(\lambda > 325 \text{ nm}, T)$ for CHBr_3 . $\alpha(532 \text{ nm})$ was measured

as part of this work and taken to be a measure of $\sigma_R(532 \text{ nm})$, i.e., assuming that CHBr_3 and sample impurities do not absorb at 532 nm. $\sigma_R(300 < \lambda < 345 \text{ nm})$ was calculated using $\sigma_R(532 \text{ nm})$ and Eq. II.

The CRDS cell used in the 532 nm extinction measurements was a 25 mm i.d. stainless steel tube with gas flow inlet and outlets at opposite ends. The gas sample filled the entire optical path and all 532 nm measurements were performed at room temperature, 296 K. The highly reflective cavity mirrors yielded ring-down time constants of $\sim 40 \mu\text{s}$ for a cavity pathlength of 95 cm. For the 300 to 345 nm region a jacketed Pyrex CRDS cell was used for temperature dependent measurements that were made simultaneously with the 532 nm measurements. The cell temperature was maintained by flowing temperature-regulated fluid from a reservoir through the jacket. A 15 cm long jacketed inlet on the cell ensured temperature equilibration of the sample before entering the optical cavity. A thermocouple in direct contact with the gas at the center of the CRD cell was used to measure the gas temperature; the temperature gradient along the length of the cell was $\leq 1 \text{ K}$. Two sets of CRDS mirrors were used to cover the wavelength range 300 to 345 nm; τ_0 values were in the range 1 to 2.5 μs for a cavity pathlength of 95 cm. The cavity mirrors were purged with a small flow of He bath gas ($\sim 8 \text{ cm}^3 \text{ s}^{-1}$, STP). The mirrors were separated from the temperature-regulated portion of the optical pathlength by $\sim 2 \text{ mm}$ diameter apertures mounted within the jacketed portion of the cell.

Experiments were performed by first recording τ_0 values at 532 nm and at a UV wavelength in the range 300 to 345 nm with only bath gas (He) flowing through the CRD cells. τ_0 values were recorded for ~ 1000 laser pulses and averaged. The precision of the individual τ_0 values was better than 1%. A CHBr_3 sample was then added to the CRDS cells and τ values were recorded and averaged. This was repeated for at least 6 different CHBr_3 concentrations in each experiment. The CHBr_3 concentration was determined using online UV absorption of CHBr_3 at 253.7 nm. The online absorption measurements used a Hg pen-ray light source and a photodiode detector. The 253.7 nm Hg line was isolated using narrow band-pass filters. The Pyrex absorption cells used had optical pathlengths of 10, 50, and 100 cm depending on the range of CHBr_3 concentrations being used, which was between $(0.2\text{--}150) \times 10^{15} \text{ molecule cm}^{-3}$. The 253.7 nm absorption cross section of CHBr_3 was taken from Gillotay et al. (1989), $1.36 \times 10^{-18} \text{ cm}^2 \text{ molecule}^{-1}$. Finally, the CRDS cells were flushed out with He bath gas and τ_0 recorded again. The τ_0 values recorded before and after the addition of CHBr_3 typically agreed to better than 0.5% and an average was used in the analysis. A linear least-squares fit of $\alpha(\lambda)$ versus $[\text{CHBr}_3]$, Eq. I, was used to determine $\sigma(\lambda, T) + \sigma_R(\lambda)$ at each wavelength.

In addition to our CHBr_3 measurements, room temperature measurements were also performed using CF_3I . The absorption cross sections of CF_3I are well-established (Solomon et al., 1994) and the measured values were used to confirm the methods used in the CHBr_3 experiments. The CF_3I concentration was measured via online UV absorption at 253.7 nm before and after the CRDS cell. The agreement with the literature $\sigma(\lambda, 298 \text{ K})$ values for CF_3I was excellent, to better than 1% at all wavelengths.

L_{Abs} was measured geometrically and also determined experimentally by comparing results from room temperature measurements performed under flow conditions using CF_3I (see (Papanastasiou et al., 2013) for additional details). A value of $L_{\text{Abs}} = 67 \pm 1 \text{ cm}$ was obtained and found to be independent of the experimental conditions that were used in the CHBr_3 experiments. This value is in good agreement with the geometric pathlength between the apertures mounted in the cell to separate the temperature jacketed and room temperature sections of the CRDS cell.

2.1 Materials

CHBr_3 (>99%) samples were degassed using freeze-pump-thaw cycles and stored under vacuum in darkened Pyrex reservoirs. Measurements performed using two different CHBr_3 samples yielded identical $\sigma(\lambda, T)$ values to within the precision of the measurements, 1.5%. In addition, identical results were obtained using CHBr_3 samples stored with or without copper turnings (a Br_2 scavenger) added to the liquid sample reservoir. As discussed later, a possible Br_2 sample impurity was found to be negligible. CHBr_3 was used pure in the majority of the experiments except for the infrared absorption measurements where gas mixtures of CHBr_3 were prepared off-line in He (UHP, 99.99%); mixtures were prepared manometrically in darkened 12 L Pyrex bulbs. Gas-phase infrared absorption spectra of the CHBr_3 samples showed no evidence of sample impurities such as commonly used stabilizers in CHBr_3 samples (ethanol ($\text{C}_2\text{H}_5\text{OH}$), amylene (1- C_5H_{10}), and epichlorohydrin ($\text{C}_3\text{H}_5\text{ClO}$) or halogenated compounds (CH_2Br_2 , CH_3Br , CHCl_2Br , CHClBr_2 , CBr_4 , and CHCl_3). The impurity upper-limits for these compounds as determined by infrared absorption would make a negligible contribution (<0.5%) to the 300-345 nm UV absorption measurements presented in this work.

Pressures were measured using calibrated 100 and 1000 Torr capacitance manometers. Total pressures in the CRD cell ranged from 80 to 180 Torr over the course of the measurements. Gas flow rates were measured with calibrated electronic mass flow meters. A total gas flow of $\sim 240 \text{ cm}^3 \text{ s}^{-1}$ (STP) was used. The linear flow velocity of the gas flowing through the CRD cells

was in the range of 4 to 7 cm s⁻¹. The uncertainty limits given throughout the paper are at the 2 σ level unless stated otherwise.

3. Results and Discussion

In this section the CHBr₃ $\sigma(\lambda,T)$ values measured in this work are presented and compared with existing literature values. A cross section parameterization is then developed for use in atmospheric models. $\sigma(\lambda,T)$ was measured between 300 and 345 nm at temperatures between 260 and 330 K and the results are summarized in Table 1 and displayed in Figure 1. The measurements performed at temperatures >296 K were included in our study primarily to improve the determination of the cross section temperature dependence, particularly for the extrapolation to lower temperatures where $\sigma(\lambda,T)$ was below our detection limit. A temperature dependence in $\sigma(\lambda,T)$ was observed at each wavelength with a decrease in $\sigma(\lambda,T)$ with decreasing temperature; the change in $\sigma(\lambda,T)$ was greatest at the longer wavelengths, as shown in Figure 1.

All of the absorption coefficient data obtained at a given wavelength (300–345 nm, 532 nm) and temperature (260–330 K) was included in a weighted linear least-squares fit to Eq. I and is available graphically in the Supplementary Material. The 532 nm extinction measurements were used to estimate the $\sigma_R(\lambda)$ contribution to the 300–345 nm extinction coefficients. Attributing $\alpha(532\text{ nm})$ entirely to Rayleigh scattering (assuming that CHBr₃ and possible impurities do not absorb significantly at 532 nm) yielded a $\sigma_R(532\text{ nm})$ value of $(3.0 \pm 0.15) \times 10^{-25}\text{ cm}^2\text{ molecule}^{-1}$. The CHBr₃ $\sigma(\lambda,T)$ values given in Table 1 were obtained by subtracting the $\sigma_R(\lambda)$ contribution which was calculated using eq II and $\sigma_R(532\text{ nm})$. $\sigma_R(\lambda)$ used in the data analysis to obtain $\sigma(\lambda,T)$ is included in Figure 1 for comparison. $\sigma_R(\lambda)$ accounted for ~20% of the measured $\alpha(345\text{ nm}, 298\text{ K})$ value and the contribution to the measured cross section value decreased toward shorter wavelengths due to the greater rate of increase in $\sigma(\lambda,T)$ than $\sigma_R(\lambda)$ at the shorter wavelengths. In the wavelength region most critical to atmospheric photolysis (<335 nm) the contribution of $\sigma_R(\lambda)$ was relatively minor, <5% (see Figure 1).

The precision and accuracy of the measured $\sigma(\lambda,T)$ values was thoroughly tested via replicate measurements as well as measurements performed using a range of experimental conditions. Overall, the precision of the measurements was high, while the uncertainty increased at longer wavelengths due to the lower $\sigma(\lambda,T)$ values and limitations imposed by the CHBr₃ vapor pressure. Uncertainties associated with the experimental parameters such as temperature and pressure made only a small contribution, <1%, to the overall uncertainty. Systematic errors

associated with the pathlength of the CRD and Hg line (253.7 nm) absorption cells were carefully examined and contributed <2% to the overall uncertainty in the $\sigma(\lambda, T)$ values reported in Table 1. Additionally tests were performed to evaluate photolytic or any other type of CHBr_3 loss through the setup and found to be negligible under the flow conditions used. The method used to extrapolate and derive $\sigma_R(\lambda)$ between 300 and 345 nm may lead to uncertainties of up to 30% in the Rayleigh scattering coefficients (Papanastasiou et al., 2013). However the correction applied to obtain the final $\sigma(\lambda, T)$ values was small. Therefore, the uncertainty associated with these corrections is estimated to be ~7% at 345 nm and less at shorter wavelengths (<3% at 330 nm).

Br_2 , which was thought to be a spectral interference in the CHBr_3 UV spectrum study of Moortgat et al. (1993), was directly probed in this work via the 532 nm CRDS measurements; the 532 nm measurements established an upper-limit to the possible contribution of a Br_2 impurity to our UV measurements. Attributing $\alpha(532 \text{ nm})$ entirely to Br_2 absorption established a 2 ppm impurity upper-limit; the Br_2 absorption cross section at 532 nm is $1.48 \times 10^{-19} \text{ cm}^2 \text{ molecule}^{-1}$ and its cross section at 345 nm is $2.05 \times 10^{-20} \text{ cm}^2 \text{ molecule}^{-1}$ (Maric et al., 1994). The 532 nm measurements establish that Br_2 made a negligible contribution to the extinction measured in the 300 to 345 nm region.

3.1 Spectrum Parameterization

The CHBr_3 absorption spectrum wavelength and temperature dependence was parameterized using the empirical expression

$$\log_{10}(\sigma(\lambda, T)) = \sum_i A_i \lambda^i + (296 - T) \sum_i B_i \lambda^i \quad (\text{III})$$

where A_i , and B_i were fit parameters. The fit included not only the $\sigma(\lambda, T)$ data given in Table 1 but also data from the Gillotay et al. (1989) and Moortgat et al. (1993) studies for wavelengths between 260 and 310 nm. Including data from these studies enabled the parameterization to be extended beyond the 300 nm short wavelength limit of the present study. The fits are included in Figure 1 and the obtained fit parameters are given in Table 2. The fit reproduces the present experimental data to within ~5% over the entire wavelength and temperature range of the measurements as shown in the bottom panel of Figure 1. The parameters given in Table 2 are appropriate for use in atmospheric model calculations. The extrapolation of the parameterization to the lower temperatures found in the upper-troposphere and lower-stratosphere yield reasonable results, but $\sigma(\lambda, T)$ should be considered less certain until verified experimentally.

3.2 Comparison with previous studies

The UV absorption spectrum of CHBr_3 has been measured previously by Gillotay et al. (1989) between 170 and 310 nm at temperatures between 240 and 295 K (low temperature measurements were made at $\lambda \leq 290$ nm) and by Moortgat et al. (1993) between 286 and 362 nm at 296, 286, 276, 266, and 256 K. The agreement of the present results with the 295 K data of Gillotay et al. at $\lambda \leq 310$ nm is good, to within 3%, as shown in the lower panel of Figure 1.

A comparison of the present $\sigma(\lambda, T)$ values with those from the Moortgat et al. (1993) study shows a systematic deviation that increases at longer wavelength and decreasing temperature. The discrepancies are quantified in the lower panel of Figure 1. Moortgat et al. reported potential problems in their measurements, particularly at the longer wavelengths, as described earlier. Although the Moortgat et al. $\sigma(\lambda, T)$ values are systematically greater than those obtained in the present work, a Br_2 impurity alone does not quantitatively explain the differences between our studies. It was also possible that CHBr_3 , which was present at high concentrations, affected the absorption cell window transmission in the Moortgat et al. study causing a systematic error in their measurements. In our work, measurements were performed using a “windowless” flow configuration. At present, there is not a clear explanation for the discrepancies observed between this work and that of Moortgat et al.

Using the CHBr_3 $\sigma(\lambda, 298 \text{ K})$ data obtained in the present work in the interpretation of the Br-atom quantum yield study of Bayes et al. (2003) would lead to an increase in their reported quantum yields. The Br-atom quantum yields in the wavelength region 300 to 324 nm would be closer but still less than unity. The reported quantum yield measurement uncertainties of 34% at 324 nm and ~10% at shorter wavelengths makes a more quantitative interpretation difficult.

4 Atmospheric Implications

The CHBr_3 $\sigma(\lambda, T)$ data reported in this study impacts its calculated atmospheric lifetime and, thus, estimates of the transport of this source gas to the stratosphere and its ODP. In this section, we briefly examine the atmospheric photolysis rate coefficient, J , of CHBr_3

$$J = \int J(\lambda) d\lambda = \int \sigma(\lambda, T) \Phi(\lambda) \Psi(\lambda, Z, \chi) d\lambda \quad (\text{IV})$$

where $\Phi(\lambda)$ is the photolysis quantum yield of CHBr_3 , which is assumed to be unity here, and $\Psi(\lambda, Z, \chi)$ is the solar flux, which is a function of λ , altitude (Z), and solar zenith angle (SZA, χ). In addition, the fractional contribution of photolysis to the total atmospheric loss of CHBr_3 , an estimate of its lifetime in the tropical region, and its estimated ODP are presented.

Seasonally averaged photolysis rate coefficients between 0 and 30 km were calculated as a function of latitude using the Tropospheric Ultraviolet and Visible (TUV) radiation model (Madronich and Flocke, 1998) available at <http://cprm.acd.ucar.edu/Models/TUV/>. The model

was run under default albedo and cloud cover conditions at 0 degrees longitude, but modified to include monthly mean pressure, temperature, and ozone climatologies available within the FAST-J photolysis model (Wild et al., 2000). These climatologies are based on measurements and model results from early stratospheric ozone assessment studies (Prather and Remsberg, 1993). Total atmospheric loss rates of CHBr_3 , i.e., photolysis + OH reactive losses, were calculated using the OH radical climatology from Spivakovsky et al. (2000). To illustrate the overall impact of the present CHBr_3 cross section data, several calculations were performed: (1) the CHBr_3 photolysis rates with the present cross section parameterization, (2) photolysis rates relative to those obtained using the current NASA/JPL recommended CHBr_3 spectrum, i.e., that of Moortgat et al. (1993), (3) an evaluation of the relative importance of including temperature dependent cross section data in the photolysis rate calculation, and (4) the fractional contribution of photolysis to the total CHBr_3 loss rate. In addition, a tropical lifetime of CHBr_3 was estimated and combined with the method developed by Brioude et al. (2010) to approximate the ODP for a very short-lived substance.

First, the wavelength dependence of the CHBr_3 photolysis rate was examined. Approximately 95% of the UV photolysis of CHBr_3 in the tropics occurs at wavelengths <335 nm; 99% for wavelengths <346 nm. Thus, the $\sigma(\lambda, T)$ measurements obtained in this work cover the most critical wavelength range for atmospheric photolysis rate calculations. Seasonally averaged CHBr_3 photolysis rates obtained using the present spectrum parameterization are shown in Figure 2. The photolysis rates show a seasonal (SZA) dependence with values in the range 0.3 to $0.7 \times 10^{-6} \text{ s}^{-1}$ in the tropical troposphere corresponding to local photolysis lifetimes of approximately 38 to 17 days with the longer local lifetimes found at the lower temperatures in the upper-troposphere.

Zonally and seasonally averaged photolysis rate vertical profiles are given in Figure 3. Figure 3 also includes the estimated range of uncertainty in the local photolysis rates. The uncertainty range was calculated from photolysis rate calculations using the 2σ minimum and maximum values in the cross section data (see Figure 1). The uncertainty in the calculated photolysis is greatest, ~14% for the Summer Tropical region, in the upper-troposphere and lower-stratosphere where the temperature is the lowest. The uncertainty in other regions is lower. It should be noted that CHBr_3 photolysis rates calculated for the low temperatures found in the upper-troposphere are dependent on the parameterization used to extrapolate the spectral data to low temperature (the experimentally measured cross section data was limited to temperatures $\geq 260 \text{ K}$). In the absence of experimental data, the extrapolation from higher temperature data may be less reliable. Direct CHBr_3 cross section measurements at

atmospherically relevant low temperatures are desirable, but were not possible using the present experimental setup. The significance of including temperature dependent cross section data is illustrated by comparison with photolysis rates calculated using only the room temperature, 298 K, CHBr_3 spectrum. The spectrum temperature dependence results in small, <10%, differences in photolysis rates below 2 km, but significant differences in the colder upper-troposphere where decreases in photolysis rates of as much as 70% are observed. A graph in the Supplementary Information shows further details of this comparison. This comparison highlights the need to include temperature dependent cross section data into models to obtain the most accurate estimate of the contribution of CHBr_3 to stratospheric bromine.

Figure 4 shows a comparison of the calculated photolysis rates obtained with the present cross section parameterization (Figure 2) and the rates obtained using the NASA/JPL recommended CHBr_3 spectrum. The systematic differences in the CHBr_3 absorption spectra are reflected in the ratio of photolysis rates shown in Figure 4. There is a weak altitude dependence observed in the ratio with values in the tropics falling in the range 0.85 to 0.9. That is, the photolysis rate in the tropical region obtained with the present spectral data is 10-15% lower (longer lifetime) than obtained using the NASA/JPL recommended values.

Figure 5 shows the relative contribution of photolysis to the overall CHBr_3 atmospheric loss rate. In this calculation, the recently reported OH + CHBr_3 reaction rate coefficient data of Orkin et al. (2013), $k(T) = 9.94 \times 10^{-13} \exp[-397/T]$, was used. This recent kinetic study reports a reaction rate coefficient that is significantly greater than recommended in NASA/JPL (Sander et al., 2011); $k(298 \text{ K, Orkin et al.})/k(298 \text{ K, NASA/JPL}) = 1.5$. A contour plot of the seasonally averaged rate coefficient ratio is included in the Supplementary Information. In addition, a comparison of the calculated total CHBr_3 loss rates obtained with our measured photolysis and the OH rate coefficient from Orkin et al. to that from the NASA/JPL values is given in the Supplementary Information. The present analysis leads to a greater overall contribution from the OH reaction loss process and a shift in the relative distribution of the loss processes from that obtained using the NASA/JPL recommended values by 15 to 20% in the tropics. Modeling studies and their associated uncertainties (Aschmann and Sinnhuber, 2013), have shown that the total CHBr_3 lifetime is a key parameter in the determination of its contribution to stratospheric ozone loss. The photolysis of CHBr_3 leads to the formation of CHBrO , while the OH radical reaction leads to the formation of CBr_2O . Both of these very short-lived products can be transported to the stratosphere (product gas injection, PGI); the estimated lifetimes of CHBrO and CBr_2O are ~ 7 and ~ 2 days, respectively (Aschmann and Sinnhuber, 2013). The modeling of PGI at present is, however, not well defined.

Evaluating the ozone depletion potential (ODP) for a very short-lived substance (VSLs) is a challenge due to the dependence on time and location of its emission. While quantifying PGI of VSLs remains uncertain, recent detailed modeling studies such as those of Hossaini et al. (2010) and Aschmann and Sinnhuber (2013) have addressed this issue. There are several modeling studies that have attempted to address the issue of the ODP for VSLs (WMO, 2007; Brioude et al., 2010; Pisso et al., 2010; Wuebbles et al., 2001) which have found that the Asian sub-continent in the Summer leads to the greatest transport of VSLs to the stratosphere. While the incorporation of the new loss process data into 3-D chemical transport models calculations is needed, the empirical relationship reported by Brioude et al. (2010) to estimate transport to the stratosphere provides a straightforward and useful method to evaluate the ODPs of VSLs (see Brioude et al. for a discussion of the assumptions applied in their analysis). Using the Brioude et al. parameterization and our total tropical region lifetime, the Indian sub-continent emission of CHBr_3 leads to a mass transfer to the stratosphere (beta) of 0.0032, 0.010, 0.022, and 0.007 using lifetimes in the tropics from this work of 13.6, 13.4, 14.3, and 13 days for Winter, Spring, Summer, and Fall (WSSF), respectively. For comparison, the tropical region lifetimes obtained using the NASA/JPL kinetic and photochemical parameters given in Sander et al. (2011) were 14.6, 14.6, 15.7, and 14.4 days (WSSF). The lifetimes calculated in this work and that obtained using the NASA/JPL parameters are similar, to within $\sim 10\%$ or less, in part, due to the offsetting effects of the revised loss processes presented in this work; the CHBr_3 photolysis lifetime increased and the OH reaction lifetime decreased. Though the lifetime calculations provide insight into the relative importance of CHBr_3 as an ozone depleting substance, we emphasize they are highly dependent on the model OH climatology and CHBr_3 vertical distribution used in the calculations. Refinement of the lifetime calculations requires a 3-D model framework that includes CHBr_3 sources and accurately predicts global OH, UV radiation, and tropopause exchange. The mass transfer for emissions from Europe, mid-latitude North America, and East Asia regions were also considered in the Brioude et al. study and were found to be considerably less effective (about one order of magnitude) in transport of VSLs to the stratosphere and, therefore, are not included in the present discussion (see Brioude et al. (2010)). The semi-empirical method reported in Brioude et al. yields CHBr_3 ODPs of 0.08, 0.26, 0.54, and 0.17 for emissions in the Indian sub-continent (WSSF). Note that due to the assumptions implemented in the approach used by Brioude et al. to calculate the ODPs, the seasonal ODP dependence is expected to be more accurate than the actual absolute values. In conclusion, CHBr_3 is a potent ozone depleting substance and the improved UV cross section data provided in

this work combined with the recent OH kinetic data from Orkin et al. (2013) enable an improved estimate of its impact on stratospheric ozone, particularly, in a changing climate.

Acknowledgements

This work was supported in part by NOAA's Climate Goal and NASA's Atmospheric Composition program.

Supplementary Material: Beer's law plots of experimental data, calculated photolysis rate dependence on temperature, OH rate coefficient change impact, change in total loss rate from new studies, plot of temperature climatology.

Table 1: CHBr₃ absorption cross sections, $\sigma(\lambda, T)$, (in units of 10^{-22} cm² molecule⁻¹, base e) measured in this work.*

λ (nm)	Temperature (K)						
	330	320	310	296	280	270	260
300	103.2 ± 3.2	92.8 ± 2.8	83.7 ± 2.0	70.4 ± 2.4	58.1 ± 1.6	53.0 ± 1.6	48.6 ± 2.6
305	52.7 ± 2.0	46.8 ± 1.8	40.8 ± 1.0	33.4 ± 1.0	27.8 ± 1.2	24.6 ± 0.8	21.6 ± 1.2
310	24.9 ± 0.8	21.4 ± 0.6	18.8 ± 0.6	15.8 ± 0.18	12.8 ± 0.4	11.2 ± 0.4	–
315	12.3 ± 0.6	10.6 ± 0.4	8.93 ± 0.4	7.02 ± 0.32	5.80 ± 0.28	4.82 ± 0.26	–
320	6.19 ± 0.4	5.14 ± 0.4	4.19 ± 0.6	3.27 ± 0.16	2.71 ± 0.12	2.46 ± 0.24	–
325	3.22 ± 0.06	2.70 ± 0.10	2.30 ± 0.06	1.63 ± 0.04	1.17 ± 0.18	–	–
330	1.60 ± 0.04	1.29 ± 0.08	1.06 ± 0.04	0.754 ± 0.020	0.515 ± 0.068	–	–
335	0.787 ± 0.034	0.626 ± 0.046	0.506 ± 0.028	0.338 ± 0.038	0.231 ± 0.052	–	–
340	0.417 ± 0.022	0.312 ± 0.028	0.240 ± 0.026	0.174 ± 0.018	0.106 ± 0.040	–	–
345	0.211 ± 0.024	0.149 ± 0.028	0.103 ± 0.018	0.0763 ± 0.0156	–	–	–

* The report uncertainties are the 2σ values from the precision of the linear least-squares fit, Beer's law, to the experimental data.

Table 2: Parameterization of the measured CHBr_3 absorption spectrum, $\sigma(\lambda, T)$, (in units of $\text{cm}^2 \text{ molecule}^{-1}$, base e) for wavelengths between 260 and 345 nm and for temperatures within the range of 260 to 330 K. In the parameterization formula, wavelength (λ) is in nm and temperature (T) is in K.

$$\log_{10}(\sigma(\lambda, T)) = \sum_i A_i \lambda^i + (296 - T) \sum_i B_i \lambda^i$$

i	A_i	B_i
0	-32.6067	0.1582
1	0.10308	-0.0014758
2	6.39×10^{-5}	3.8058×10^{-6}
3	-7.7392×10^{-7}	9.187×10^{-10}
4	-2.2513×10^{-9}	-1.0772×10^{-11}
5	6.1376×10^{-12}	—

Figure Captions

Figure 1 UV absorption spectrum of CHBr_3 (bromoform). Upper panel: Experimental results from this work for temperatures between 260 and 330 K (see legend). The solid lines are values calculated using the parameterization given in Table 2; the dotted lines represent the parameterization in regions where there is no experimental data; the dashed line is the CHBr_3 Rayleigh scattering cross section used in the data analysis. Lower panel: Percent residual of the difference between the experimental data and the parameterization given in the upper panel, $\text{Residual} = 100 \times (\text{Exp} - \text{Par})/\text{Par}$. The filled circles are from this work (see legend in upper panel). Experimental data from previous studies are included for comparison (see legend). Note that the residuals for the Moortgat et al. (1993) study have been divided (scaled downward) by a factor of 5 for clarity. The data error bars are 2σ of the measurement uncertainty.

Figure 2 Calculated seasonally averaged CHBr_3 photolysis rate coefficients (in units of 10^{-6} s^{-1}) obtained using the UV absorption cross section parameterization given in Table 2. Photolysis rates were calculated using the NCAR TUV code (Madronich and Flocke, 1998) with temperature, pressure, and ozone climatologies available within the FAST-J photolysis model (Wild et al., 2000) (see text for details). Regions where photolysis rate coefficients were calculated to be zero are shown as white space.

Figure 3 Summary of CHBr_3 seasonally averaged photolysis rate vertical profiles for the tropics, mid-, and polar regions. The shaded regions represent the 2σ range of photolysis rate calculated using the $\pm 2\sigma$ estimated uncertainty in the CHBr_3 UV absorption cross section data (see Figure 1 and Table 1). For the tropics, only the Summer and Winter profiles with the Summer uncertainty are shown for improved figure clarity.

Figure 4 Ratio of the calculated seasonally averaged CHBr_3 photolysis rates obtained using the CHBr_3 UV spectrum parameterization from this work (Table 2) and those obtained using the NASA/JPL (Sander et al., 2011) spectrum recommendation (i.e., the spectrum data from Moortgat et al. (1993)). Photolysis rates were calculated as in Figure 2 (see text). Regions where the photolysis rate coefficients were calculated to be zero are shown as white space.

Figure 5 Calculated seasonally averaged fractional loss of CHBr_3 due to UV photolysis. CHBr_3 photolysis rates were calculated using the UV spectrum parameterization from this work (Table

2) as in Figure 2. The OH rate coefficient data was taken from Orkin et al. (2013) and the OH climatology from Spivakovsky et al. (2000) (see text). Note that the OH climatology is only available up to 17 km. Regions where either the calculated photolysis rate coefficient or OH concentration were calculated to be zero are shown as white space.

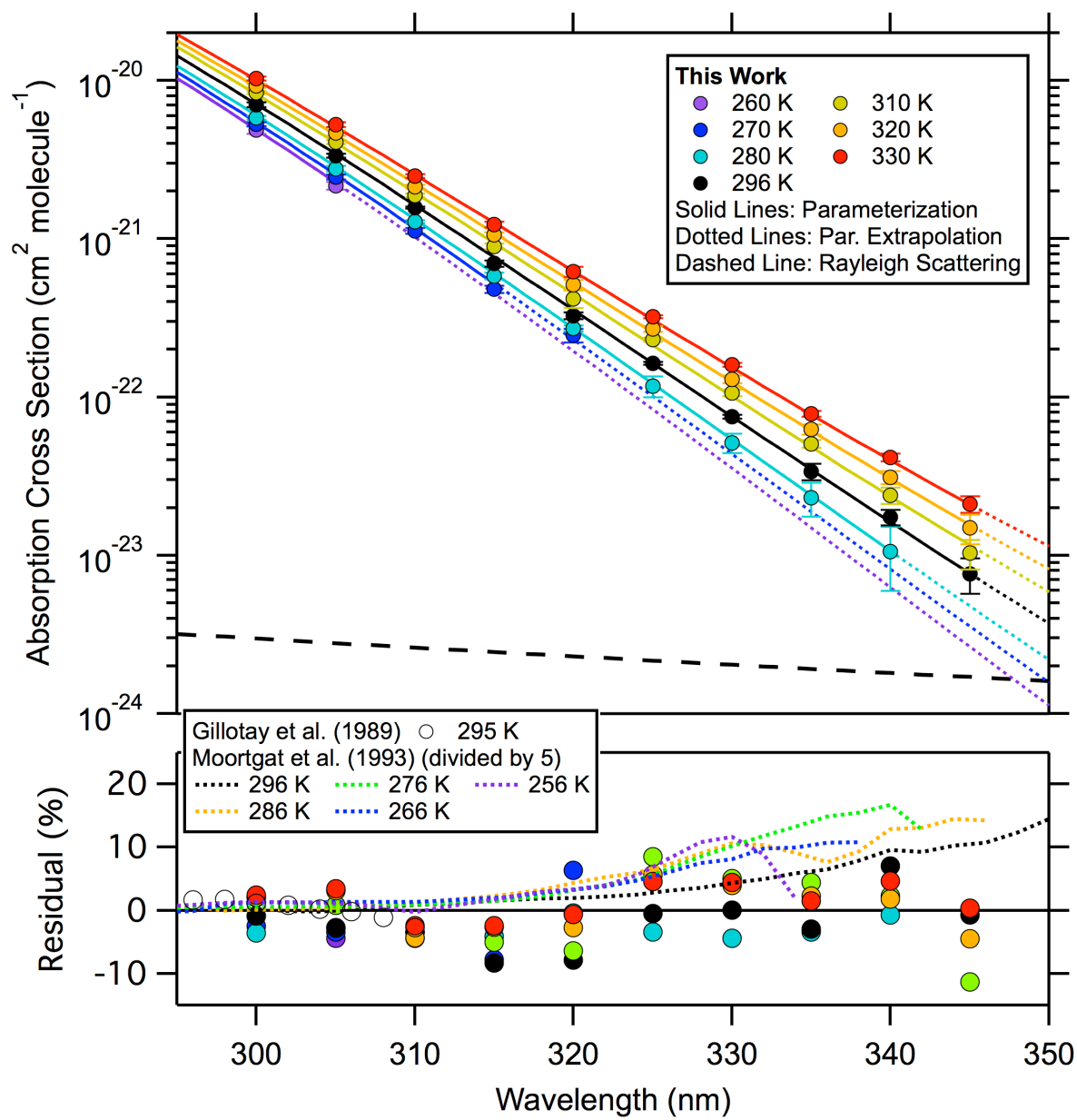


Figure 1

CHBr₃ Photolysis Rate

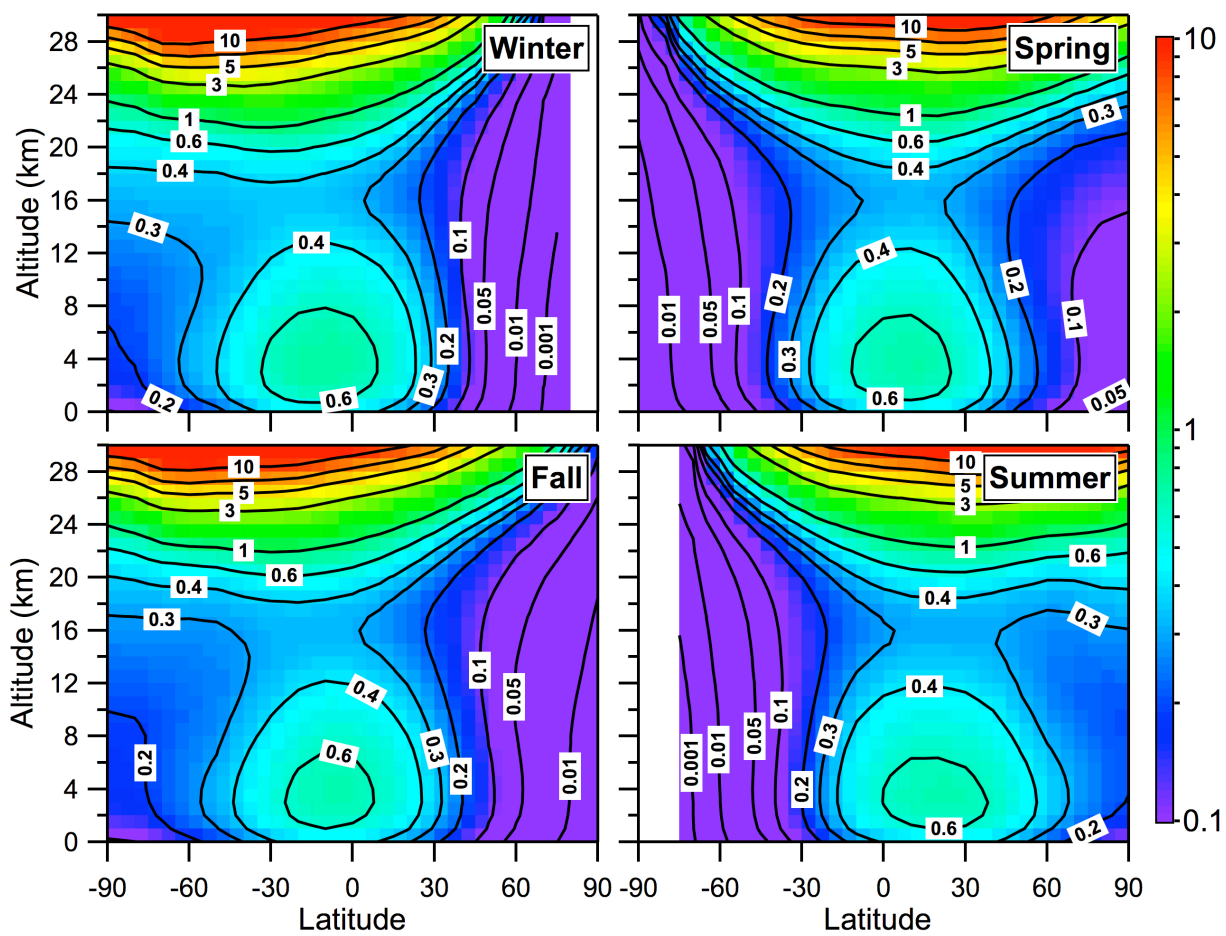


Figure 2

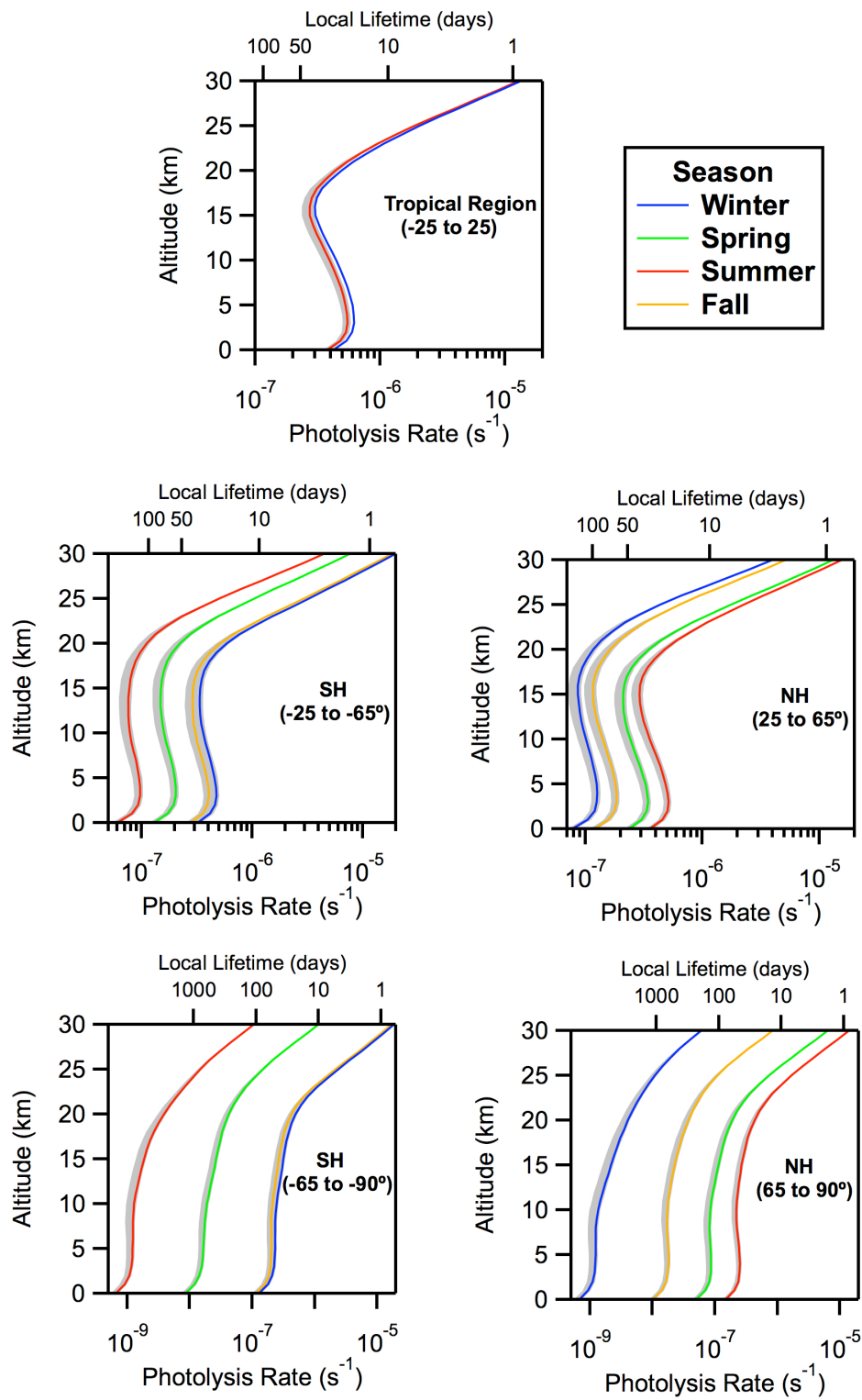


Figure 3:

CHBr₃ Photolysis Rate: This Work / JPL10-6

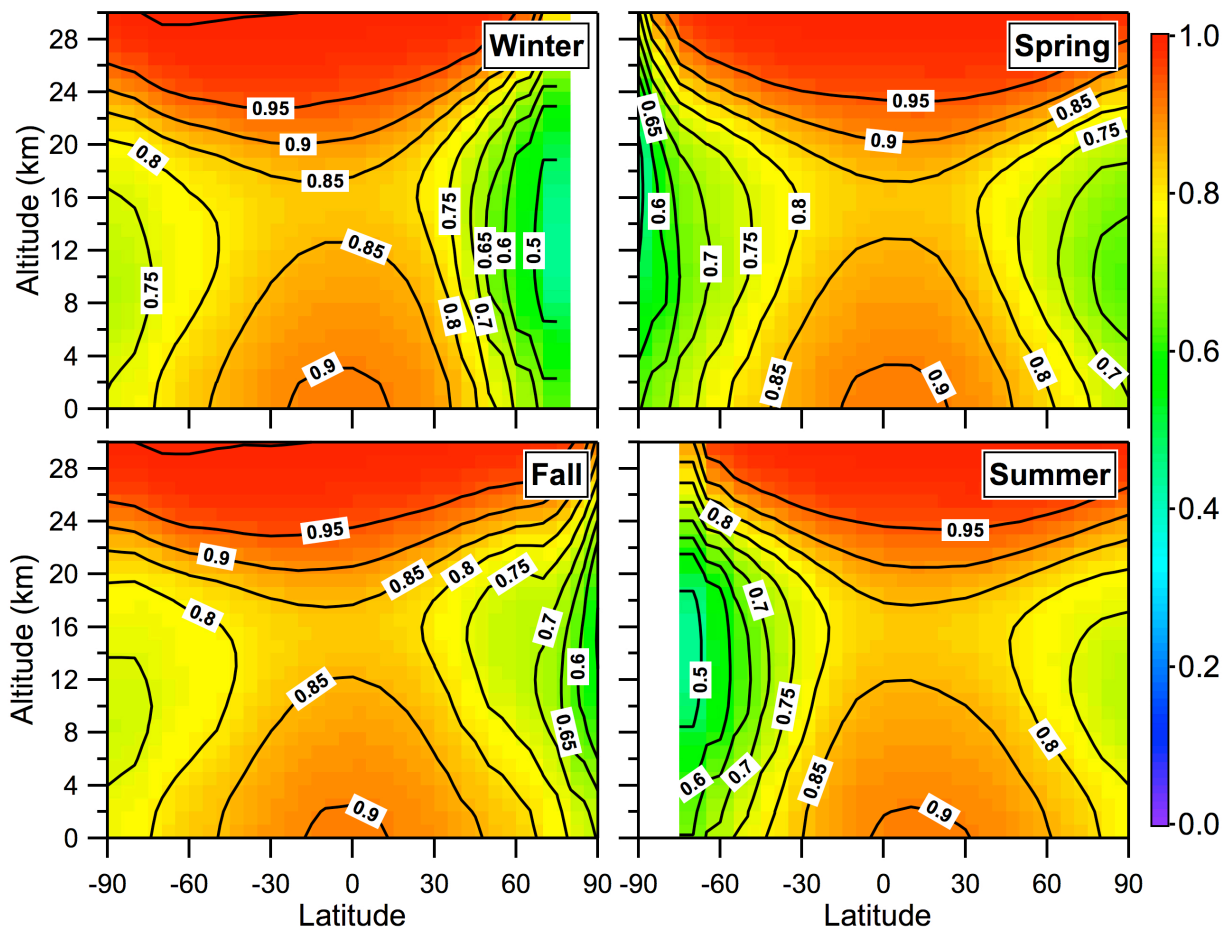


Figure 4

CHBr₃ Fractional Photolysis Loss: $J(T) / (J(T) + k[OH])$

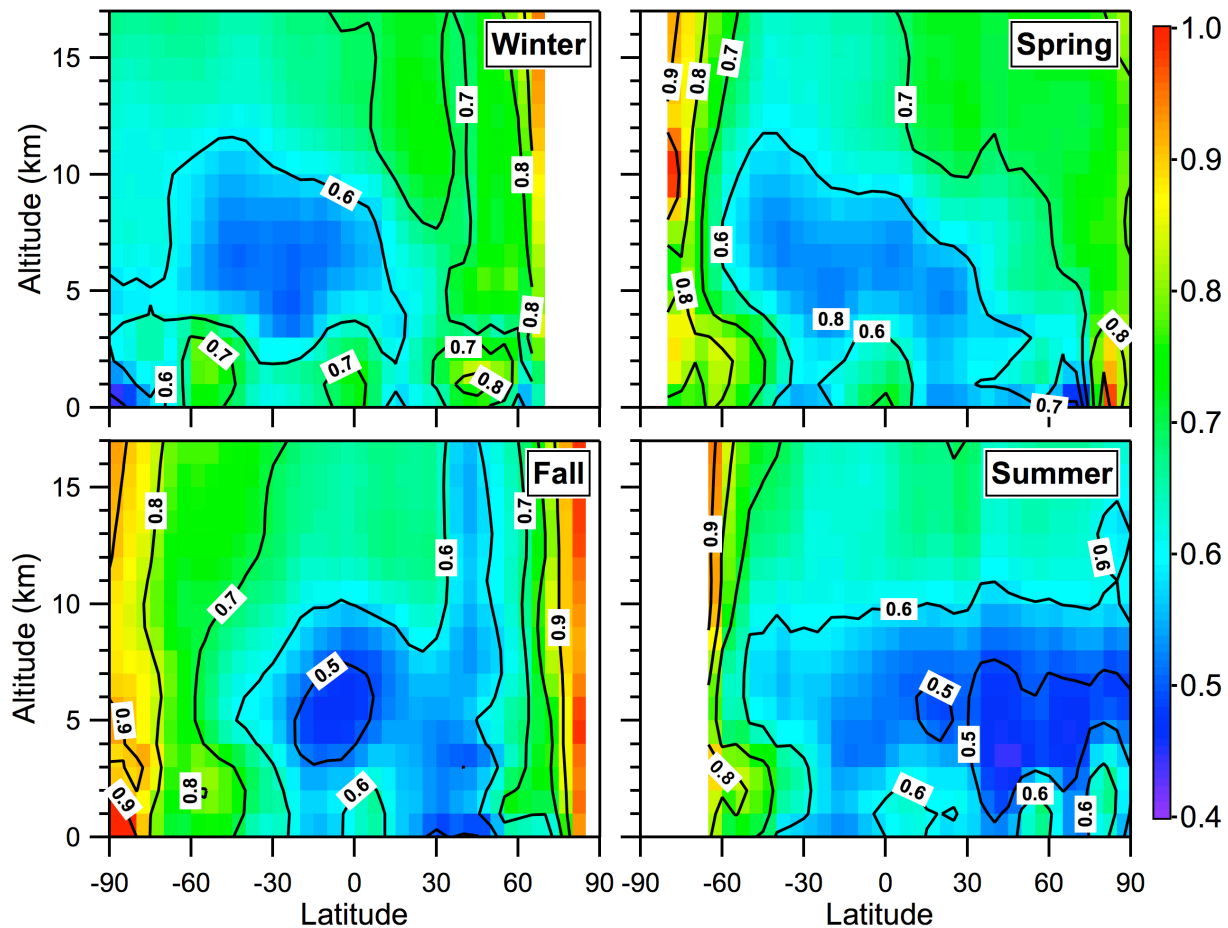


Figure 5

References

- Aschmann, J., and Sinnhuber, B.-M.: Contribution of very short-lived substances to stratospheric bromine loading: uncertainties and constraints, *Atmos. Chem. Phys.*, 13, 1203-1219, doi:10.5194/acp-13-1203-2013, 2013.
- Bayes, K. D., Friedl, R. R., Sander, S. P., and Toohey, D. W.: Measurements of quantum yields of bromine atoms in the photolysis of bromoform from 266 to 324 nm, *J. Geophys. Res.*, 108, doi:10.1029/2002JD002877, 2003.
- Brioude, J., Portmann, R. W., Daniel, J. S., Cooper, O. R., Frost, G. J., Rosenlof, K. H., Granier, C., Ravishankara, A. R., Montzka, S. A., and Stohl, A.: Variations in ozone depletion potentials of very short-lived substances with season and emission region, *Geophys. Res. Lett.*, 37, L19804, doi: 10.1029/2010GL044856, 2010.
- Feierabend, K. J., Flad, J. E., Brown, S. S., and Burkholder, J. B.: HCO quantum yields in the photolysis of HC(O)C(O)H (Glyoxal) between 290 and 420 nm, *J. Phys. Chem. A*, 113, 7784-7794, 2009.
- Gillotay, D., Jenouvrier, A., Coquart, B., Merienne, M. F., and Simon, P. C.: Ultraviolet Absorption Cross-Sections of Bromoform in the Temperature Range 295-240 K., *Planet. Space Sci.*, 37, 1127-1140, 1989.
- Hossaini, R., Chipperfield, M. P., Monge-Sanz, B. M., Richards, N. A. D., Atlas, E., and Blake, D. R.: Bromoform and dibromomethane in the tropics: a 3-D model study of chemistry and transport, *Atmos. Chem. Phys.*, 10, 719-735, 2010.
- Huang, H.-Y., Chuang, W.-T., Sharma, R. C., Hsu, C.-Y., Lin, K.-C., and Hu, C.-H.: Molecular elimination of Br₂ in 248 nm photolysis of bromoform probed by using cavity ring-down absorption spectroscopy, *J. Chem. Phys.*, 121, 5253-5260, 2004.
- Madronich, S., and Flocke, S. The role of solar radiation in atmospheric chemistry. In *Handbook of Environmental Chemistry*; Boule, P., Ed.; Springer-Verlag: Heidelberg, 1998; pp 1-26.
- Maric, D., Burrows, J. P., and Moortgat, G. K.: A study of the UV-visible absorption spectra of Br₂ and BrCl, *J. Photochem. Photobiol. A: Chem.*, 83, 179-192, 1994.
- Moortgat, G. K., Meller, R., and Schneider, W. Temperature dependence (256-296 K) of the absorption cross-sections of bromoform in the wavelength range 285-360 nm. In *The tropospheric chemistry of ozone in the polar regions*; Niki, H., Becker, K. H., Eds.; Springer-Verlag Berlin Heidelberg, 1993; Vol. 17.
- O'Keefe, A., and Deacon, D. A. G.: Cavity ring-down optical spectrometer for absorption measurements using pulsed laser sources, *Rev. Sci. Instr.*, 59, 2544-2551, 1988.
- Orkin, V. L., Khamaganov, V. G., Kozlov, S. N., and Kurylo, M. J.: Measurements of rate constants for the OH reactions with bromoform (CHBr₃), CHBr₂Cl, CHBrCl₂, and epichlorohydrin (C₃H₅ClO), *J. Phys. Chem. A*, doi: 10.1021/jp3128753, 2013.
- Papanastasiou, D., Rontu Carlon, N., Neuman, J. A., Fleming, E. L., Jackman, C. H., and Burkholder, J. B.: Revised UV Absorption Cross Sections of CF₂Br₂, CF₂ClBr, and CF₂BrCF₂Br and Ozone Depletion Potentials, *Geophys. Res. Lett.*, 40, doi: 10.1002/GRL.50121, 2013.
- Peterson, K. A., and Francisco, J. S.: Should bromoform absorb at wavelengths longer than 300 nm?, *J. Chem. Phys.*, 117, 6103-6107, 2002.
- Pisso, I., Haynes, P. H., and Law, K. S.: Emission location dependent ozone depletion potentials for very short-lived halogenated species, *Atmos. Chem. Phys.*, 10, 12025-12036, doi:10.5194/acp-10-12025-2010, 2010.
- Prather, M. J., and Remsberg, E. E. (eds), 1993, The atmospheric effects of stratospheric aircraft: Report of the 1992 stratospheric models and measurements workshop, NASA, Ref. Publ., 1292, p. 672.

- Sander, S. P., Abbatt, J., Barker, J. R., Burkholder, J. B., Friedl, R. R., Golden, D. M., Huie, R. E., Kolb, C. E., Kurylo, M. J., Moortgat, G. K., Orkin, V. L., and Wine, P. H.: Chemical Kinetics and Photochemical Data for Use in Atmospheric Studies, Evaluation Number 17, JPL Publication 10-6, 2011. <http://jpldataeval.jpl.nasa.gov>.
- Solomon, S., Burkholder, J. B., Ravishankara, A. R., and Garcia, R. R.: Ozone depletion and global warming potentials of CF₃I, *J. Geophys. Res.*, 99, 20929 - 20935, 1994.
- Spivakovsky, C. M., Logan, J. A., Montzka, S. A., Balkanski, Y. J., Foreman-Fowler, M., Jones, D. B. A., Horowitz, L. W., Fusco, A. C., Brenninkmeijer, C. A. M., Prather, M. J., Wofsy, S. C., and McElroy, M. B.: Three-dimensional climatological distribution of tropospheric OH: Update and evaluation, *J. Geophys. Res.*, 105, 8931-8980, 2000.
- Wild, O., Zhu, X., and Prather, M. J.: FAST-J: accurate simulation of in- and below-cloud photolysis in tropospheric chemical models, *J. Atmos. Chem.*, 37, 245–282, 2000.
- WMO (World Meteorological Organization), *Scientific Assessment of Ozone Depletion: 2006*, Global Ozone Research and Monitoring Project-Report No. 50, 572 pp., Geneva, Switzerland, 2007.
- WMO (World Meteorological Organization), *Scientific Assessment of Ozone Depletion: 2010*, Global Ozone Research and Monitoring Project-Report No. 52, 516 pp., Geneva, Switzerland, 2011.
- Wuebbles, D. J., Patten, K. O., Johnson, M. T., and Kotamarthi, R.: New methodology for ozone depletion potentials of short-lived compounds: n-Propyl bromide as an example, *J. Geophys. Res.*, 106, 14551-14571, 2001.
- Xu, D., Francisco, J. S., Huang, J., and Jackson, W. M.: Ultraviolet photodissociation of bromoform at 234 and 267 nm by means of ion velocity imaging, *J. Chem. Phys.*, 117, 2578-2585, 2002.